Naval Research Laboratory

Washington, DC 20375-5320

NRL/MR/5310--14-9553

A Computer Model for Bistatic Sea Surface Microwave Reflectivity

Rashmi Mital
Vilhelm Gregers-Hansen

Radar Analysis Branch
Radar Division

August 14, 2014

REPORT DOCUMENTATION PAGE

Form Approved
OMB No. 0704-0188

1. REPORT DATE *(DD-MM-YYYY)*	**2. REPORT TYPE**	**3. DATES COVERED** *(From - To)*
14-08-2014	Memorandum Report	October 2009 – October 2010

4. TITLE AND SUBTITLE

A Computer Model for Bistatic Sea Surface Microwave Reflectivity

5a. CONTRACT NUMBER

5b. GRANT NUMBER

5c. PROGRAM ELEMENT NUMBER

6. AUTHOR(S)

Rashmi Mital and Vilhelm Gregers-Hansen

5d. PROJECT NUMBER
53-6018-0-15

5e. TASK NUMBER

5f. WORK UNIT NUMBER
6018

7. PERFORMING ORGANIZATION NAME(S) AND ADDRESS(ES)

Naval Research Laboratory
4555 Overlook Avenue, SW
Washington, DC 20375-5320

8. PERFORMING ORGANIZATION REPORT NUMBER

NRL/MR/5310--14-9553

9. SPONSORING / MONITORING AGENCY NAME(S) AND ADDRESS(ES)

Naval Research Laboratory
4555 Overlook Avenue, SW
Washington, DC 20375-5320

10. SPONSOR / MONITOR'S ACRONYM(S)

11. SPONSOR / MONITOR'S REPORT NUMBER(S)

12. DISTRIBUTION / AVAILABILITY STATEMENT

Approved for public release; distribution is unlimited.

13. SUPPLEMENTARY NOTES

14. ABSTRACT

This report describes an approach for calculating the bistatic microwave reflectivity of the sea surface for transmit and receive grazing angles less than 10 degrees and any relative geometry through 360 degrees. In the forward scatter region, including specular and glistening zone, the model relies on the work of Beckman and Spizzichino supplemented with later work on shadowing [2] and polarization effects [3]. Outside the forward scatter region, the model is heuristic and based on the similarities between measured monostatic and bistatic sea reflectivity. The motivation behind the model described is the evaluation of the magnitude of jamming reflections into the radar main beam and sidelobes from the sea surface. Such jamming reflections, which sometimes are referred to as "hot clutter," can degrade the performance of adaptive jamming cancellation systems. The model also applies to evaluation of the performance of bistatic radar systems. The complete model is incorporated in a single MATLAB® function call, used as a basis for a graphic user interface (GUI), which provides a useful tool to analyze a wide range of scenarios. This code is described in two appendixes and will be provided to qualified organizations upon request.

15. SUBJECT TERMS

16. SECURITY CLASSIFICATION OF:			**17. LIMITATION OF ABSTRACT**	**18. NUMBER OF PAGES**	**19a. NAME OF RESPONSIBLE PERSON**
a. REPORT	**b. ABSTRACT**	**c. THIS PAGE**			Rashmi Mital
Unclassified Unlimited	Unclassified Unlimited	Unclassified Unlimited	Unclassified Unlimited	40	**19b. TELEPHONE NUMBER** *(include area code)* (202) 767-2584

Standard Form 298 (Rev. 8-98)
Prescribed by ANSI Std. Z39.18

CONTENTS

1 INTRODUCTION

This report describes an approach for calculating the bistatic microwave reflectivity of the sea surface. This report will only address low grazing angles, as encountered with shipboard radar systems, but include both in-plane and out-of-plane geometries. Higher grazing angles as well as airborne or space-based radars will need additional models.

In the forward scatter region the model is based on the work of Beckman and Spizzichino [1] supplemented with later work on shadowing [2] and polarization effects [3]. Outside the forward scatter glistening zone, the model is heuristic and based on similarities between measured monostatic and bistatic reflectivities. The main objective of the model described here is to evaluate the magnitude of jamming reflections into the radar main beam and sidelobes from the sea surface. Such jamming reflections, sometimes referred to as "hot clutter", can degrade the performance of adaptive jamming cancellation systems such as sidelobe cancellers. The model would also apply to the evaluation of the performance of bistatic radar systems.

Under standard propagation conditions, bistatic reflections via the sea surface for a remote transmitted signal into a receive antenna will exist at all azimuth angles out to the 4/3 earth radar horizon associated with either transmitter or receiver heights. During ducting conditions, reflections can occur from longer ranges dependent on the refractive properties of the atmosphere. The effects of ducting could most likely be accounted for in the model using a procedure similar to that proposed by Dockery [4] for monostatic sea clutter. This approach relies on propagation predictions obtained from a program such as TEMPER [5]. This generalization is not included in the present work.

2 BISTATIC RECEIVED POWER

The bistatic power reflected from a given radar resolution cell is proportional to the product of the resolution cell area (A_c) and the normalized bistatic reflectivity (σ_B^0) of the sea surface for a given geometry. The bistatic reflectivity has the non-dimensional unit of bistatic radar cross-section per unit surface area (m^2/m^2). The received bistatic power further takes into account the transmitted power, the gain of both transmit and receive antennas, and the one-way propagation factors from the transmit antenna to the reflecting area on the surface and from here to the receive antenna.

For non-cooperative scenarios, such as noise jamming, the resolution cell area is defined by the intersection of transmit and receive beams. Pulse jamming will additionally need to consider the spatial extent of the pulse length. For cooperative systems, such as bistatic radar, the resolution cell area is further limited by the surface area contained within iso-range and iso-doppler contours associated with the range and Doppler resolution of the system. In cases where the resolution cell area is so large that the

Manuscript approved June 3, 2014.

reflection coefficient varies spatially within the cell, the cell must be subdivided and contributions non-coherently summed to calculate the total average power.

The superposition of three physical processes describes bistatic sea reflectivity. These are (1) coherent scatter (reflection) from the specular region, (2) strong diffuse scatter from the glistening region, and (3) wide angle diffuse scatter from the sea surface outside the glistening region. Figure 1 shows these three regions for an antenna located on a Navy ship. The results apply only to the sea surface inside the 4/3 earth horizon for both transmitter and receiver. Figure 1a shows the volume of the three physical processes described earlier. Figure 1b shows an example of the glistening zone.

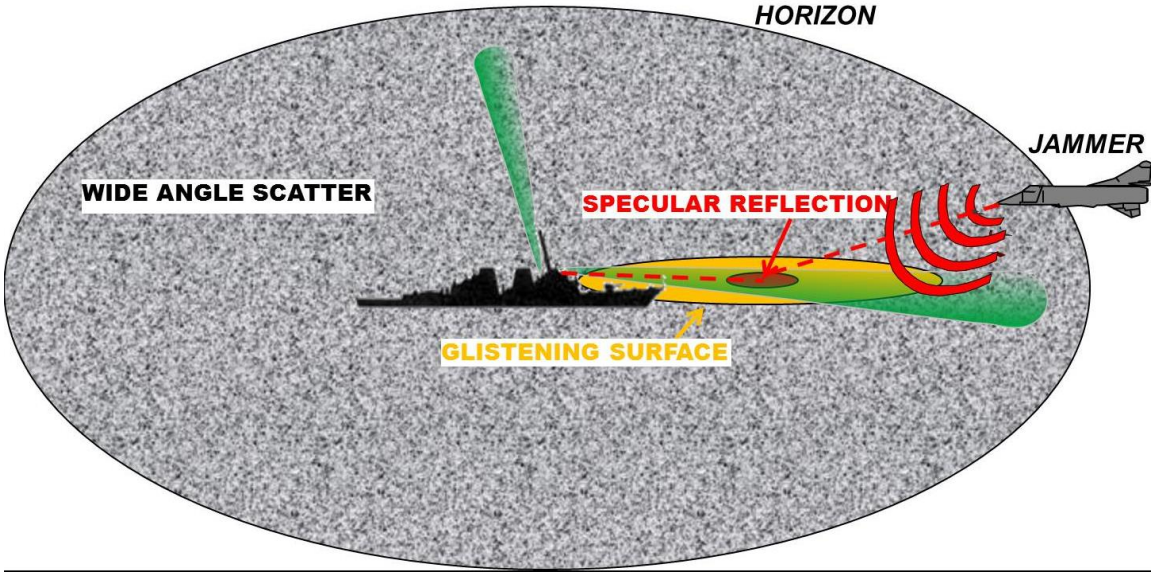

Figure 1a: The three physical processes for bistatic sea reflectivity

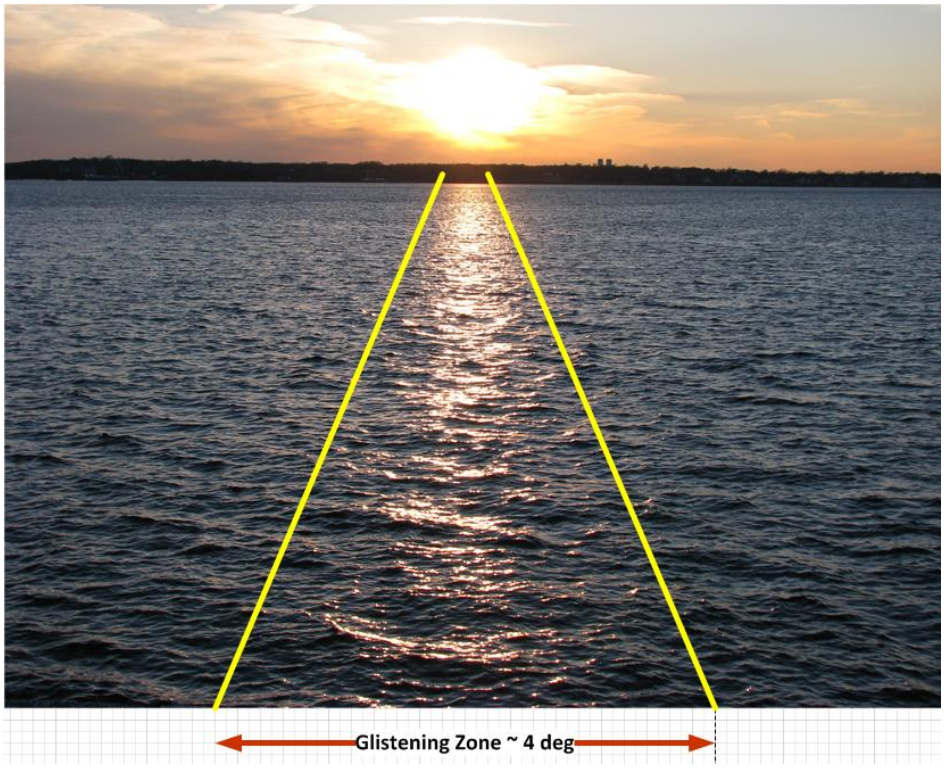

Figure 1b: An example of a glistening zone

Specular forward scatter from the sea-surface will result in coherent multipath interference while diffuse forward scatter will produce non-coherent scatter. This report discusses each of these three forms of scatter and combines them into a MATLAB® script used to calculate the surface reflectivity for arbitrary geometries. Each of the three cases uses a different mathematical model.

2.1 Specular Scatter

Specular scatter comes from a small region on the surface around the specular point (see Fig. 1a) at which the incidence and reflection angles are equal and located in the vertical plane including both transmitter and receiver. The effect of standard refraction by the atmosphere is taken into account by using an effective earth radius R_e = 8500 km instead of the actual radius of the earth. The range loss associated with the total path length, from the source to the specular point, and from here to the receiver, together with the coherent reflection coefficient of the surface determines the complex amplitude of the received specular reflected signal. In addition, the gain of the transmitter and receiver antennas must also be taken into account.

The coherent reflection coefficient, ρ_c is

$$\rho_C = \rho_o \cdot \rho_S \cdot D \qquad (1)$$

In Eq. (1), ρ_o is the Fresnel reflection coefficient for sea water for either horizontal or vertical polarization, ρ_S is the additional rough-surface specular reflection coefficient, and *D* is the divergence factor (see p.245 in [1]). For the bistatic model addressed here, the divergence is assumed to be unity.

The Fresnel reflection coefficients can be calculated using classical EM (electromagnetic) equations (see p. 218-219 in [1]). The Fresnel reflection coefficient for horizontal polarization is:

$$\rho_0^H = \frac{\sin\gamma - \sqrt{Y^2 - \cos^2\gamma}}{\sin\gamma + \sqrt{Y^2 - \cos^2\gamma}} \qquad (2)$$

and for the vertical polarization.

$$\rho_0^V = \frac{Y^2\sin\gamma - \sqrt{Y^2 - \cos^2\gamma}}{Y^2\sin\gamma + \sqrt{Y^2 - \cos^2\gamma}} \qquad (3)$$

In these equations, *Y* is the electrical impedance of the surface:

$$Y = \sqrt{\frac{\varepsilon_{rc}}{\mu_{rc}}} \qquad (4)$$

where μ_{rc} is the relative permeability (≈ 1) and ε_{rc} is the complex dielectric constant defined as:

$$\varepsilon_{rc} = \varepsilon_r - j60\lambda\sigma \qquad (5)$$

Here ε_r is the relative permittivity of the sea surface assumed to be 80 (see p.219 in [1]), λ is the wavelength in meters and, σ is the conductivity of the surface in mho/m.

The angle γ is the grazing angle of the incident field. For specular scatter, the grazing angle for the incident field is equal to the grazing angle of the reflected field. As the sea surface gets rougher, the specular component reflects smaller amounts of the EM energy. The rough surface specular reflection coefficient, ρ_S quantifies this phenomenon. The rough surface specular reflection coefficient depends on the root-mean-square (rms) wave height, σ_h, the wavelength of operation, λ, and the grazing angle, γ. For a Gaussian sea surface model, the rms rough surface specular reflection coefficient is given by (eq.246 in [1]):

$$\rho_S = \exp\left[-\frac{1}{2}\left(\frac{4\pi\sigma_h\sin\gamma}{\lambda}\right)^2\right] \qquad (6)$$

Using Eq. (6), Fig. 2 shows the specular coefficient for various sea states. When sea state is zero, the reflection coefficient is one and it drops rapidly as the sea state increases. This plot is at X-band (10 GHz). Section 2.2.1 describes the Gaussian sea surface model in more detail.

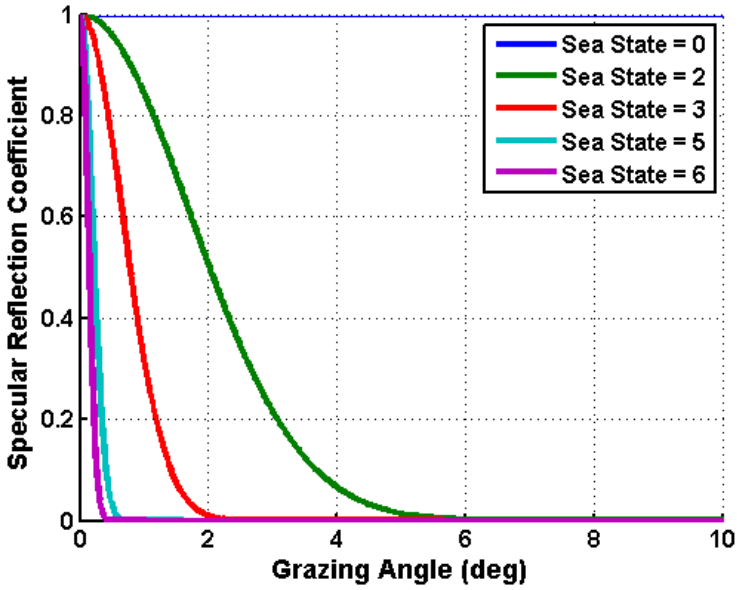

Figure 2: Specular reflection coefficient vs. grazing angle for different sea states

2.2 Diffuse Scatter

Diffuse scattering occurs over an extended region of the sea surface. The primary contribution is from a region known as the "glistening surface" (p.250 in [1]). The glistening surface is assumed to consist of small wave facets (presumed larger than radar wavelength), which act as mirrors and each of which is oriented such that the transmitter reflects an incoming EM field towards the receiver. Figure 3 illustrates such diffuse scattering. In Fig. 3, any wave facet with the correct slope and orientation reflects the EM energy toward the receiver. If the slope is not correct, then this energy is scattered in other directions.

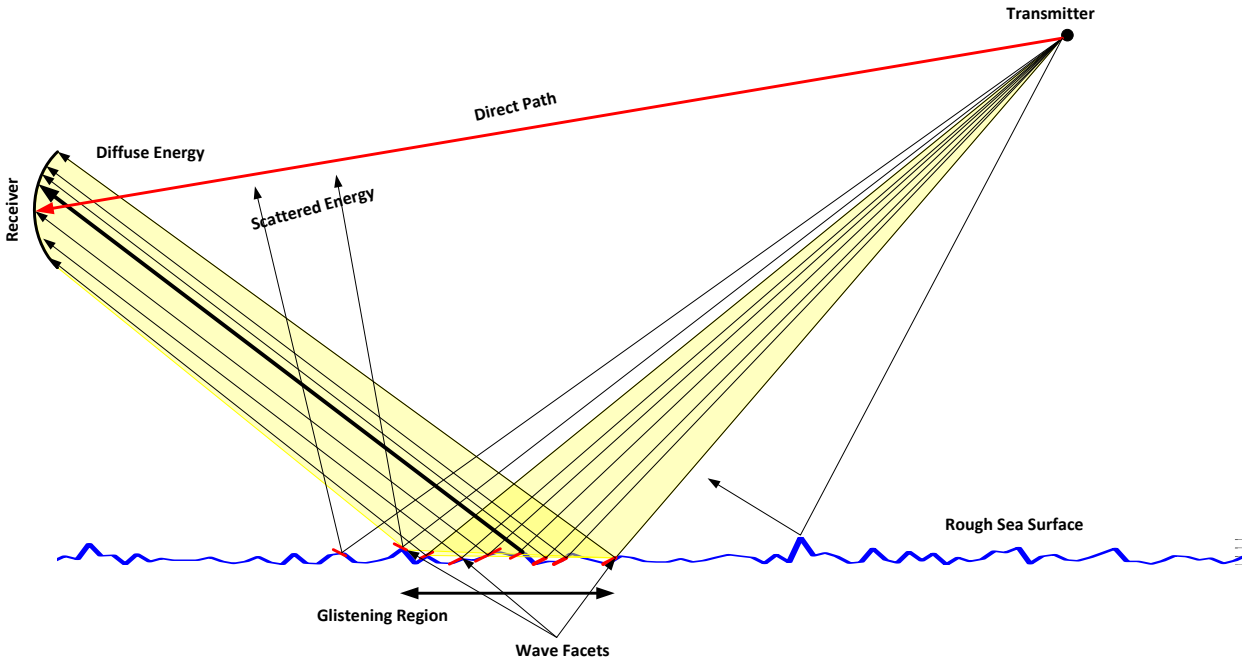

Figure 3: Diffuse scattering

2.2.1 Sea Surface Model

The model assumes that the rough sea surface lies in the x-y plane with the height of the rough surface in the z-direction. The rough sea surface is then modeled as a two-dimensional Gaussian random surface according to Beckmann and Spizzichino (p. 80, eq.(2) in [1]). The term $\zeta(x,y)$ defines the sea surface where ζ is the wave height relative to the mean at coordinate (x,y). The resulting Normal probability density function of the wave height is defined by the rms (root-mean-square) value of the wave-height, σ_h, and is given by

$$p(\zeta) = \frac{1}{\sqrt{2\pi}\sigma_h} \exp\left(-\frac{\zeta^2}{2\sigma_h^2}\right) \qquad (7)$$

The rms wave height σ_h is ¼ of the significant wave height which is defined as the average of the one-third highest waves at the given sea state. Table 1 shows the definition of sea states as provided by the World Meteorological Organization (WMO) and the related significant wave heights, rms wave height, and correlation distance.

The autocorrelation function for the two-dimensional Gaussian random surface is assumed to be Gaussian and is defined by (p.81 in [1]):

$$C(\tau) = \exp\left(-\frac{\tau^2}{T^2}\right) \qquad (8)$$

In eq. (8), T represents the "correlation distance" of the waves. For this model, the value of T is usually much larger than the wavelength of the radar. The model assumes that the correlation distance is the same in all directions. Table 1 also includes the correlation distance T assumed for the different sea states. An example of the Gaussian sea surface model based on equations (7-8) is shown in Fig. 4.

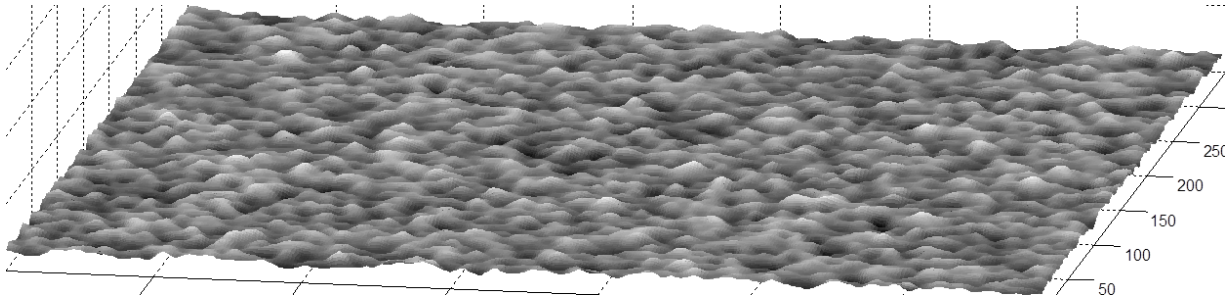

Figure 4: Simulated Gaussian sea surface model

2.2.2 Diffuse Scatter Reflectivity

As previously described, the direction and amplitude of the reflected wave assumes that the sea surface between the receiver and transmitter is entirely composed of small plane elements (also referred to as facets). Each of these facets acts as a mirror. The distribution of the slopes of these mirrors will have a normal distribution with a zero mean and a standard deviation defined as the rms wave slope, ς_0. Based on the Gaussian surface model of the sea, it can be shown that the rms wave slope is given by the rms value of the wave height σ_h and the correlation distance T according to (p.251 in [1]):

$$\varsigma_0 = \tan\beta_0 = \frac{2\sigma_h}{T} \qquad (9)$$

This equation also defines the angle, β_0, corresponding to the rms slope. Due to the symmetry of the sea surface model the rms wave slope is the same in all directions. The "glistening surface" is the region from which the transmitter reflects significant power of the incident EM wave into the receiver by facets with the appropriate slope and direction. Table 1 lists the rms wave slopes for the different sea states.

Table 1: Sea States Wave Height, Correlation Distance, and RMS Wave Slope

WMO Sea State	Significant Wave Height(m)	Characteristics	RMS Wave Height σ_h (m)	Correlation Distance T(m)	RMS Wave Slope, ς
0	<0.04	Calm	~0.01	0.40	0.05
1	0.04-0.1	Calm (ripples)	0.03	0.47	0.12
2	0.1-0.5	Smooth	0.11	1.61	0.14
3	0.5-1.25	Smooth	0.29	3.92	0.15
4	1.25-2.5	Moderate	0.59	7.41	0.16
5	2.5-4.0	Rough	1.03	11.42	0.18
6	4.0-6.0	Very Rough	1.61	14.68	0.22
7	6.0-9.0	High	2.37	18.96	0.25

2.2.3 Normalized Bistatic RCS

In Beckmann and Spizzichino, [1] an equation was derived for the bistatic RCS based on an evaluation of the statistical properties of the wave slope for a given transmitter/receiver geometry. However, this equation did not consider the effects of surface reflectivity, polarization, and shadowing. To include all of these effects, the product of the three terms defines the normalized bistatic RCS as:

$$\sigma_0^B(x,y) = G\left(\beta(x,y)\right)\cdot S(x,y)\cdot\left|\rho(x,y)\right|^2 \qquad (10)$$

In Eq. (10), $G\left(\beta(x,y)\right)$ accounts for the wave-slope statistics (the classical Beckmann and Spizzichino equation), *S(x, y)* accounts for shadowing, and $\rho(x, y)$ represents the reflectivity and polarization effects of the individual wave facets.

The term $G\left(\beta(x,y)\right)$ accounts for the wave-slope statistics at a surface cell whose location is given by its x- and y- coordinates. Assuming that the rough sea surface is modeled as a two-dimensional

Gaussian random surface, Beckmann and Spizzichino have obtained the expected value of the reflectivity as a function of the required slope of the facet, β, and the rms wave-slope, β_0, as (p.252 in [1]):

$$G(\beta) = \frac{1}{\tan^2(\beta_0)\cdot\cos^4(\beta)} \exp\left[-\frac{\tan^2(\beta)}{\tan^2(\beta_0)}\right] \qquad (11)$$

The required slope β, is the angle between the bisector angle of the incident and scattered rays and the z-axis of the surface as shown in Figure 5.

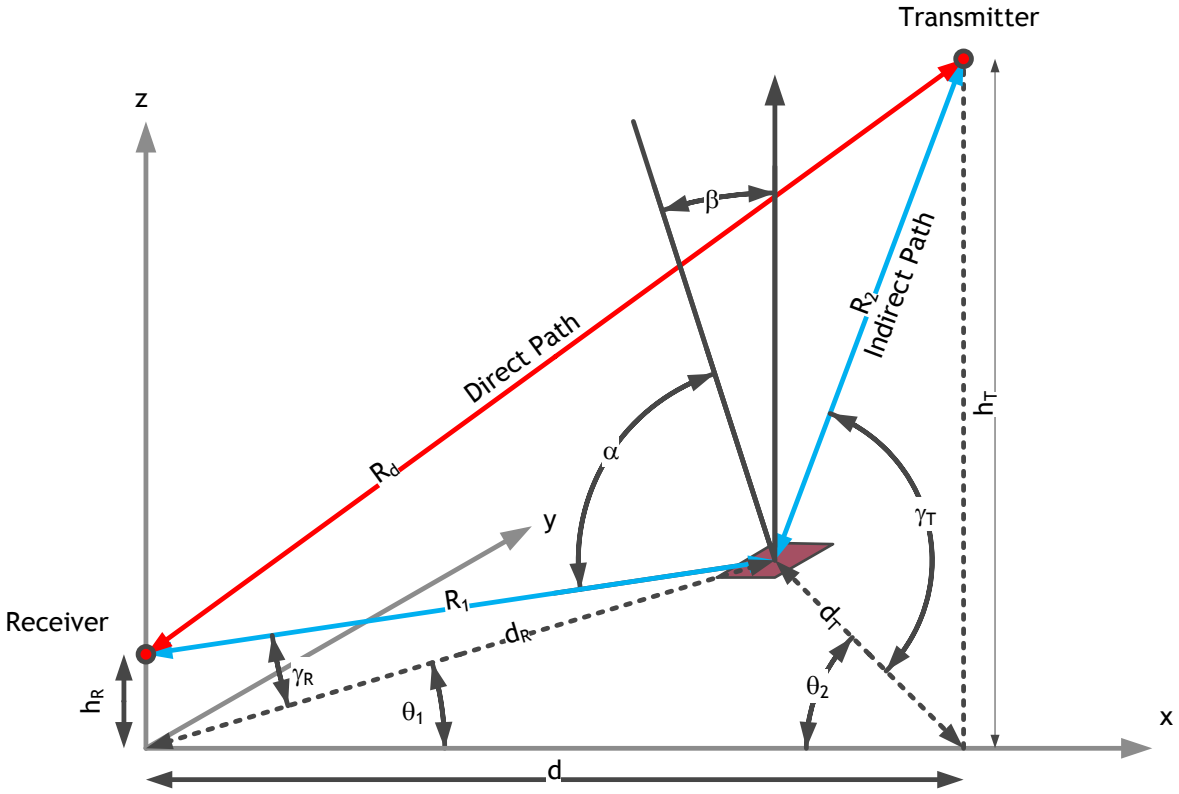

Figure 5: Geometry Used for the Calculation of Wave-Slope Dependence Factor

To calculate the bisector angle, β, assume that the receiver is located at the origin with a finite height of h_R and the transmitter is located at a distance d away at height h_T. The x-y-z coordinates are defined such that the reflecting cell and the receiver are always located on the x-axis. The angle γ_R and γ_T are the grazing angles of the receiving and transmitting paths with the x-y plane. The bisector angle can be determined in terms of the receiver grazing angle, the transmitter grazing angle and the sum of the off axis angle of the transmitter θ_2 and off axis angle of the receiver θ_1 as

$$\tan\beta = \frac{\sqrt{\cos^2(\gamma_T) - 2\cos(\gamma_T)\cos(\gamma_R)\cos(\theta) + \cos^2(\gamma_R)}}{\sin(\gamma_R) + \sin(\gamma_T)} \qquad (12)$$

where the angle θ is the sum of the angles θ_1 and θ_2.

In the case of a curved earth, the grazing angles are calculated with respect to the horizontal at the reflecting cell as discussed by Blake (pp.254-257 in [6]). Figures 6a, b and c show the curved earth geometry for the three paths – d (surface path between receiver and transmitter), d_T (surface path between transmitter and reflecting cell) and d_R (surface path between the receiver and the reflecting cell).

Considering the geometry of Figure 6a, the angle θ_d relates the height of the transmitter and the height of the receiver by

$$h_T = \frac{(R_e + h_R) \times \sin(\theta_d + \frac{\pi}{2})}{\sin(\pi - (\theta_d + \frac{\pi}{2}) - \phi)} - R_e \qquad (13)$$

where the angle ϕ is measured at the center of the earth and is equal to $\frac{d}{R_e}$.

The path lengths R_1 and R_2 together form the indirect path while the path length R_d is the length of the direct path. The path lengths R_1 and R_2 can be calculated using the geometry shown in Figures 6b and 6c as

$$R_1 = \sqrt{h_R^2 + 4 \times R_e \times (R_e + h_R) \times \sin^2\left(\frac{\phi_1}{2}\right)}$$
$$R_2 = \sqrt{h_T^2 + 4 \times R_e \times (R_e + h_T) \times \sin^2\left(\frac{\phi_2}{2}\right)} \qquad (14)$$

where

$$\phi_1 = \frac{d_R}{R_e}$$
$$\phi_2 = \frac{d_T}{R_e} \qquad (15)$$

An indirect path between a receiver, transmitter and a reflecting cell will be possible only by establishing a line of sight between the three points.

Finally, the grazing angles γ_R and γ_T can be calculated using the geometries in Figures 2b and c respectively. Since the distances in the y-direction are small, the angle θ can be accurately determined using flat earth geometry.

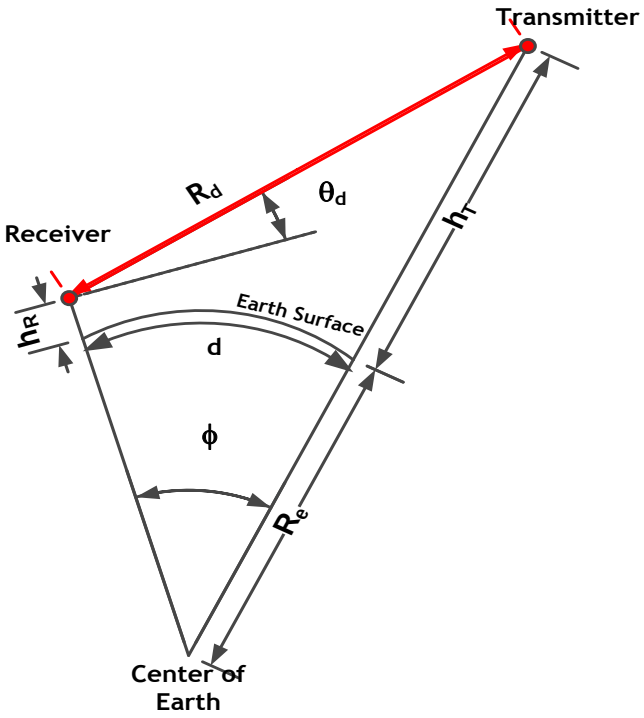

Figure 6a: Curved Earth Geometry when the Surface Path (*d*) between Receiver and Transmitter is considered

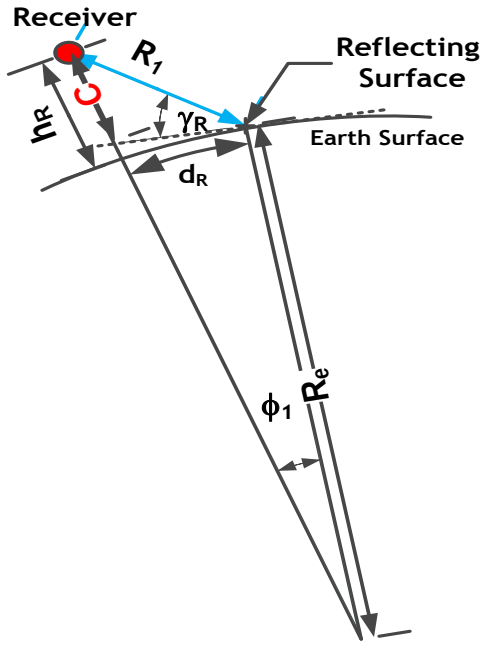

Figure 6b: Curved Earth Geometry when the Surface Path (d_R) between Receiver and Reflecting Cell is considered

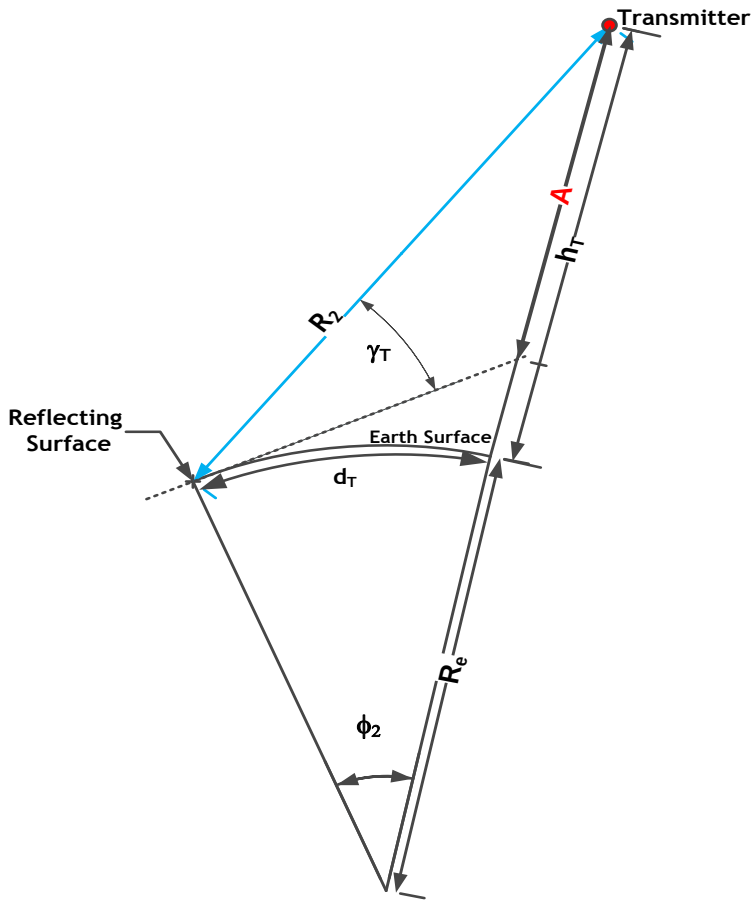

Figure 6c: Curved Earth Geometry when Surface Path (d_T) between Transmitter and Reflecting Cell is considered

The term $\rho(x,y)$ calculates the reflectivity of the wave facet (reflecting cell) located at coordinates x, y. This term includes the change in polarization due to reflection of a tilted surface. The reflectivity of a wave facet is given by (eq.18 in [3]):

$$\rho_{VV} = \frac{a_2 a_3}{\sin^2(2\alpha)}\rho_0^V\left(\frac{\pi}{2}-\alpha\right)+\frac{\cos(\gamma_R)\cos(\gamma_T)\sin^2(\theta)}{\sin^2(2\alpha)}\rho_0^H\left(\frac{\pi}{2}-\alpha\right)$$
$$\rho_{HV} = \frac{a_3\cos(\gamma_T)\sin(\theta)}{\sin^2(2\alpha)}\rho_0^V\left(\frac{\pi}{2}-\alpha\right)-\frac{a_2\cos(\gamma_R)\sin(\theta)}{\sin^2(2\alpha)}\rho_0^H\left(\frac{\pi}{2}-\alpha\right)$$
$$\rho_{VH} = -\frac{a_3\cos(\gamma_T)\sin(\theta)}{\sin^2(2\alpha)}\rho_0^H\left(\frac{\pi}{2}-\alpha\right)+\frac{a_2\cos(\gamma_R)\sin(\theta)}{\sin^2(2\alpha)}\rho_0^V\left(\frac{\pi}{2}-\alpha\right)$$
$$\rho_{HH} = \frac{a_2 a_3}{\sin^2(2\alpha)}\rho_0^H\left(\frac{\pi}{2}-\alpha\right)+\frac{\cos(\gamma_R)\cos(\gamma_T)\sin^2(\theta)}{\sin^2(2\alpha)}\rho_0^V\left(\frac{\pi}{2}-\alpha\right) \qquad (16)$$

where the first subscript is the polarization of the scattered signal and the second subscript is the polarization of the incident signal and the parameters ρ_0^V and ρ_0^H are the Fresnel reflection coefficients as described in Section 2.1 . In section 2.1 ρ_0^V and ρ_0^H were calculated at the grazing angle, γ, which was the grazing angle with respect to the horizontal. In this case, the grazing angle will be determined from the angle α which is the angle between the bisector and either the incident or the reflected ray. It can be calculated in terms of the grazing angles and the off-axis angle of the transmitter as:

$$\cos(\alpha) = \sqrt{\frac{1 - \cos(\gamma_R)\cos(\gamma_T)\cos(\theta) + \sin(\gamma_R)\sin(\gamma_T)}{2}} \qquad (17)$$

Note, that Eq. (16) considers a general case where polarization of the transmitted beam can change as it scans in azimuth (electronically scanned array). For example, at boresight, a vertical beam is truly vertical but as the main beam scans, some of the energy will leak into the orthogonal polarization (horizontal). Thus, the second terms in Eq. (16) are to include the effects of these cross pol terms. The geometrical parameters a_2 and a_3 are:

$$\begin{aligned} a_2 &= \cos(\gamma_R)\sin(\gamma_T) + \sin(\gamma_R)\cos(\gamma_T)\cos(\theta) \\ a_3 &= \cos(\gamma_T)\sin(\gamma_R) + \sin(\gamma_T)\cos(\gamma_R)\cos(\theta) \end{aligned} \qquad (18)$$

2.2.4 Shadowing Effects

Neglecting shadowing effects, when considering scattering of EM waves from rough surfaces, can result in errors, as the power due to diffuse scattering will be overestimated. Several papers such as Smith [7] and Wagner [2] have addressed this issue. According to these authors the simplest way of including shadowing of a rough surface is to introduce a shadowing factor *S(x,y)* at the location of the reflecting facet.

For there to be no shadowing, a given facet has to be "visible" to both the receiver and the transmitter. Otherwise, the reflecting cell will be shadowed and will not contribute to diffuse scattered power. Figure 7 shows a ray being shadowed. This discussion implies the assumption that geometrical optics provides a valid mathematical approach. Presently, there is no known approach that takes diffraction into account. The equations to calculate shadowing have been derived from Smith (eqs.20-25 [7]) and Bourlier (eqs.5a,49 in [8]) and are one-dimensional in nature. These equations are dependent only on the slopes of the rays from the receiver and the transmitter but are independent of the heights of the waves:

$$S(x,y) = \frac{(1+erf(v_R)) \times (1+erf(v_T))}{4(1+\Lambda_R + \Lambda_T)} \qquad (19)$$

where

$$v_k = \frac{|\tan(\gamma_k)|}{\sqrt{2}\tan\beta_0}$$
$$\Lambda_k = \frac{e^{-v_k^2} - v_k\sqrt{\pi}erfc(v_k)}{2v_k\sqrt{\pi}} \qquad (20)$$

In this equation, k corresponds to either the transmit path (T) or the receive path (R).

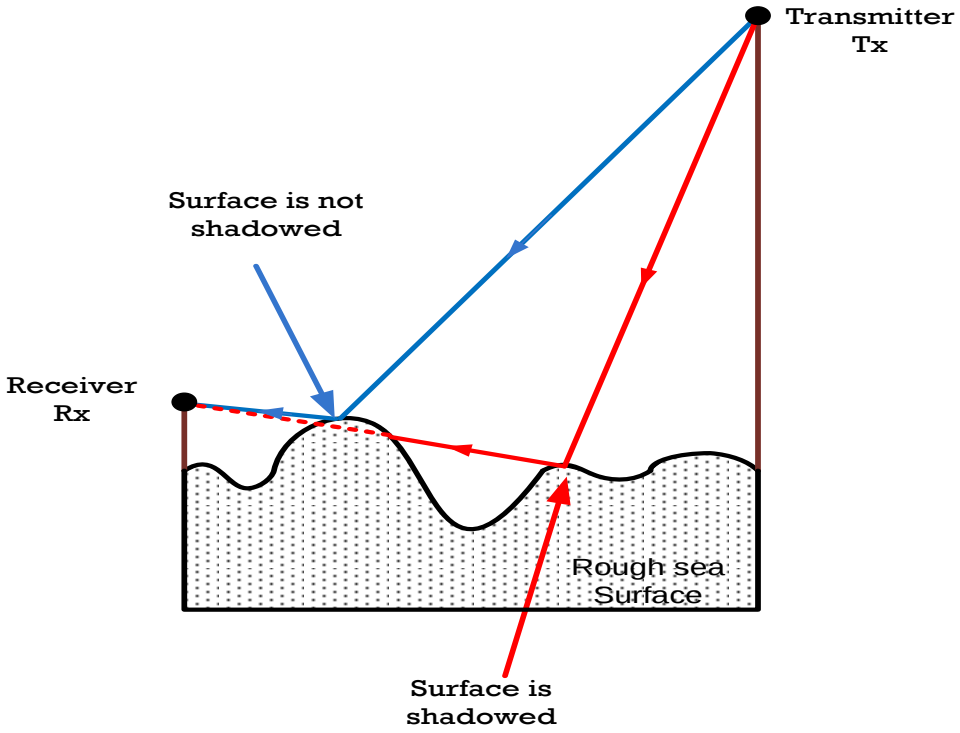

Figure 7: Effect of Shadowing

Using Eq. (19-20), the shadowing factor is plotted vs. incident grazing angle for three different transmit grazing angles of 1^o, 5^o and 10^o. These plots show that shadowing decreases with increasing transmit and receive grazing angles. This means that there is higher probability of a given resolution cell being "seen" by both the transmitter and receiver. Also at higher sea states, the shadow factor is larger. Once again, higher sea states mean increased wave heights and hence an increased probability of a surface cell being shadowed.

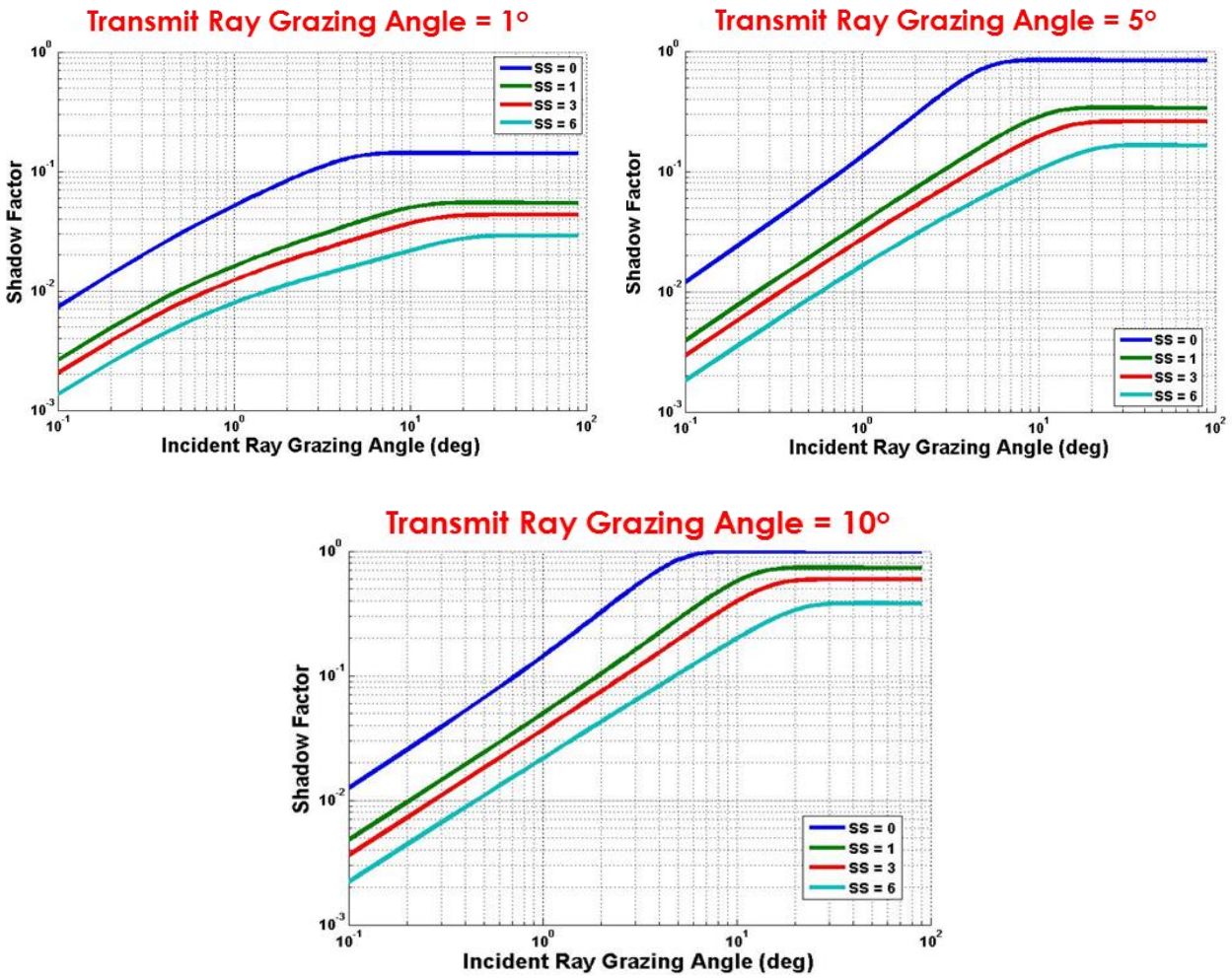

Figure 8: Shadowing function vs. incident grazing angle for three different transmit ray-grazing angles

2.2.5 Wide Angle Scatter

In addition to the forward reflection caused by specular reflection and scattering from the glistening surface, diffuse scattering occurs at wide angles outside the glistening surface. This is the result of, capillary waves, spray, and breaking waves, and the mechanisms are similar to those causing monostatic sea clutter returns. In this bistatic model, the wide-angle scattering is determined simply by calculating the monostatic RCS for the smaller of the two grazing angles on transmit and receive – γ_T or γ_R. The maximum of the contributions from the glistening surface or the wide-angle scattering determines the normalized bistatic RCS for any azimuth angle. The normalized bistatic RCS for wide-angle scattering is calculated using an empirical equation [9] based on the Nathanson tables of experimental data [10]. The bistatic RCS for the vertical or horizontal polarizations for the given reflecting cell is:

$$\sigma_{V,H}^{M}\,(dB) = c_1 + c_2 \times \log_{10}\left(\sin\left[\min\left(\gamma_R,\gamma_T\right)\right]\right) + \frac{\left(27.5 + c_3 \times \left[\min\left(\gamma_R,\gamma_T\right)\right]\right) \times \log_{10} f}{1 + 0.95 \times \left[\min\left(\gamma_R,\gamma_T\right)\right]} + c_4 \times (1+SS)^{\frac{1}{2+0.085\times\left[\min\left(\gamma_R,\gamma_T\right)\right]+0.033\times SS}} + c_5 \cdot \left[\min\left(\gamma_R,\gamma_T\right)\right] \qquad (21)$$

where γ_T and γ_R are the grazing angles (in deg) determined in Section 2.2.3 , SS is the sea state and f is the operating frequency of the radar in GHz.

Then for wide angle scatter

$$\sigma_{WA}^{0} = \max\left(\sigma_0^B, \sigma^M\right)_{V,H} \qquad (22)$$

The five parameters for the calculation of the RCS for the horizontal and vertical polarizations are:

Table 2: Constants Used in Empirical Sea Clutter Model

Constants	**Polarization**	
	Horizontal	**Vertical**
c_1	-73.0	-50.79
c_2	20.78	25.93
c_3	7.351	0.7093
c_4	25.65	21.58
c_5	0.0054	0.00211

Figure 9 plots the empirical sea clutter model equations and compares them with the points from Nathanson's [10] experimental data. The results shown are for S-band (3.0 GHz) for sea states ranging from zero to six and grazing angles varying from 0.1-90 deg. Analysis has shown that the mean absolute deviation between Nathanson's tables and Eq. (21) is less than 2.3 dB [11].

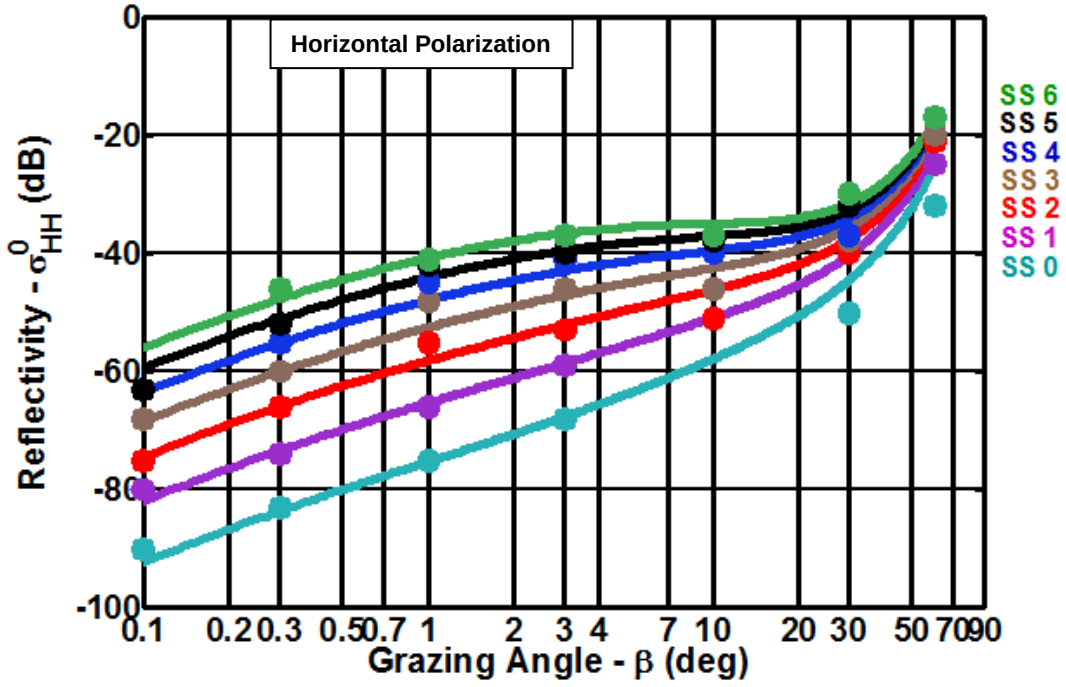

(a)

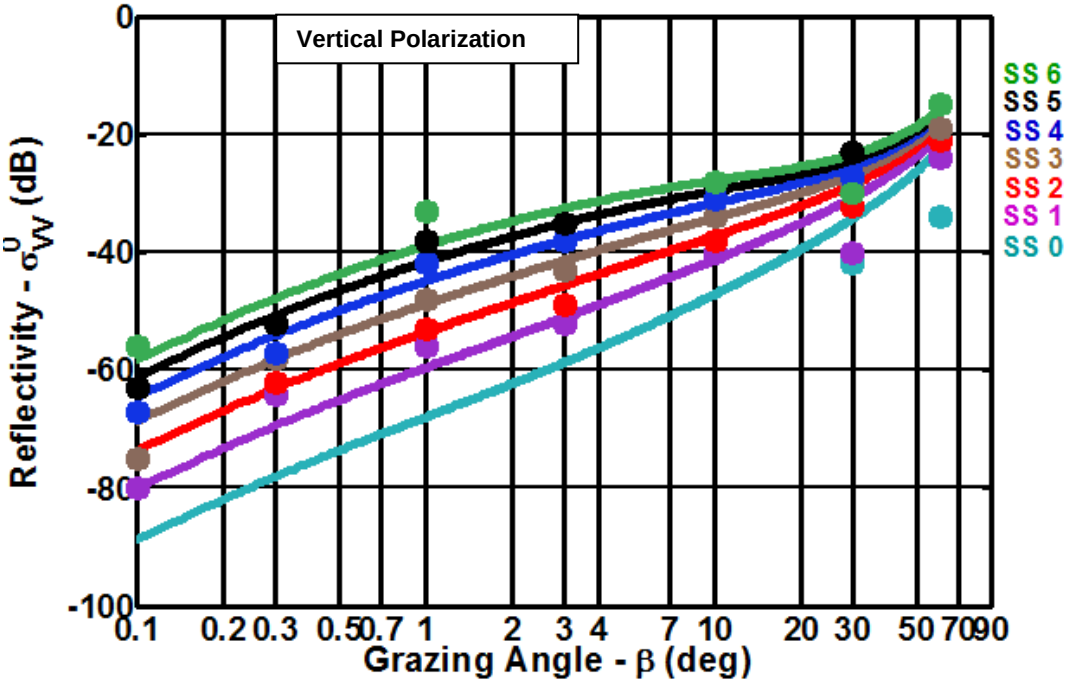

(b)

Figure 9: Comparison of empirical vs. experimental data for (a) horizontal and (b) vertical polarization

2.2.6 Examples

Using the equations summarized in the earlier sections, some numerical examples are shown in the following. These results were obtained using the MATLAB® program described in the Appendix. In

addition to the total bistatic surface reflectivity, results are also obtained showing the time delay distribution of power reflected into the receiving antenna. Such time delays play an important role in determining the maximum jamming cancellation that can be achieved with a given adaptive architecture.

Figure 10 plots the bistatic reflectivity of the glistening zone over a surface area of 10 km X 300 m. The receiver antenna is at a height of 20 m while the transmitter has a height of 225 m above the surface. The transmitter has an isotropic gain. The receiver has a beamwidth of $2^o \times 2^o$ at S-band (3 GHz). All results are normalized to the gain of the receiver. The sidelobes of the receive antenna are 40 dB below the main beam. The sea state is three. In the example shown in Fig. 10, neither shadowing nor wide-angle scatter is included.

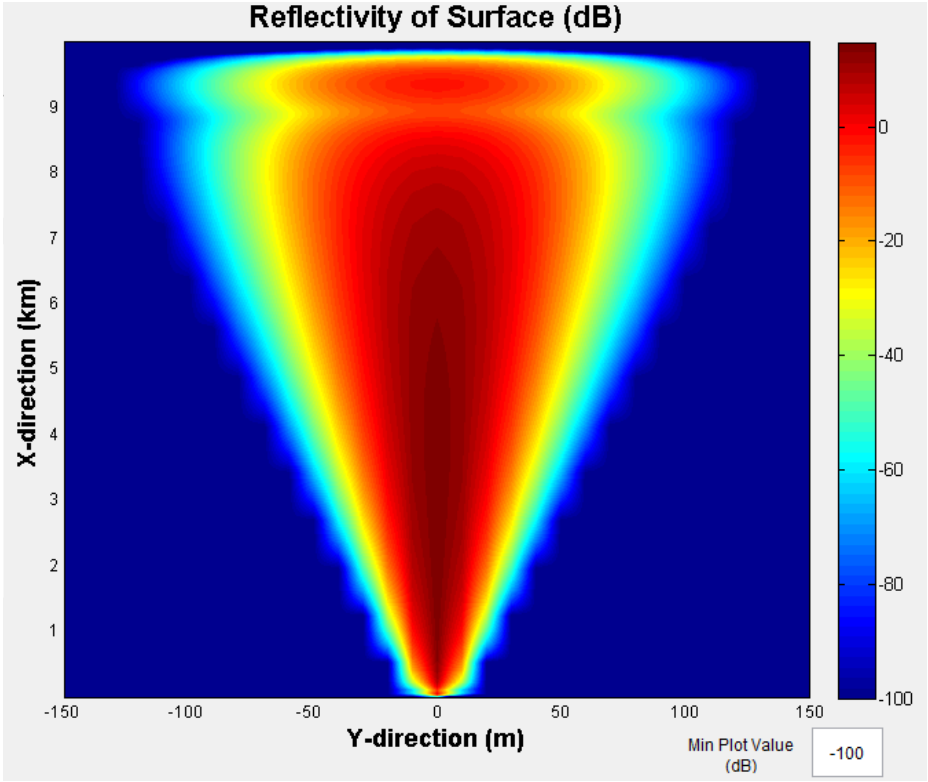

Figure 10: Example of bistatic reflectivity from glistening zone

Since the glistening area is quite large, reflections from the surface have a distribution in time. Power from surface can reach the receiver at from times as short as a couple of nanoseconds to times in hundreds of nanoseconds and even microseconds. Figure 11a shows an example of the distribution of time over the surface by drawing isolines (in time) of 10, 20, 30 and 40 ns. In this example, the reflections from the edge of the glistening zone will take more than 40 ns to reach the receiver. To draw a plot of power vs. time, sum the reflected power bound by regions of equal time. Using this technique, Fig. 11b plots of the

power distribution vs. time and cumulative power distribution vs time. A similar technique, using isolines in range, allow forming a plot power distribution vs. range. Appendix B shows an example of a range plot.

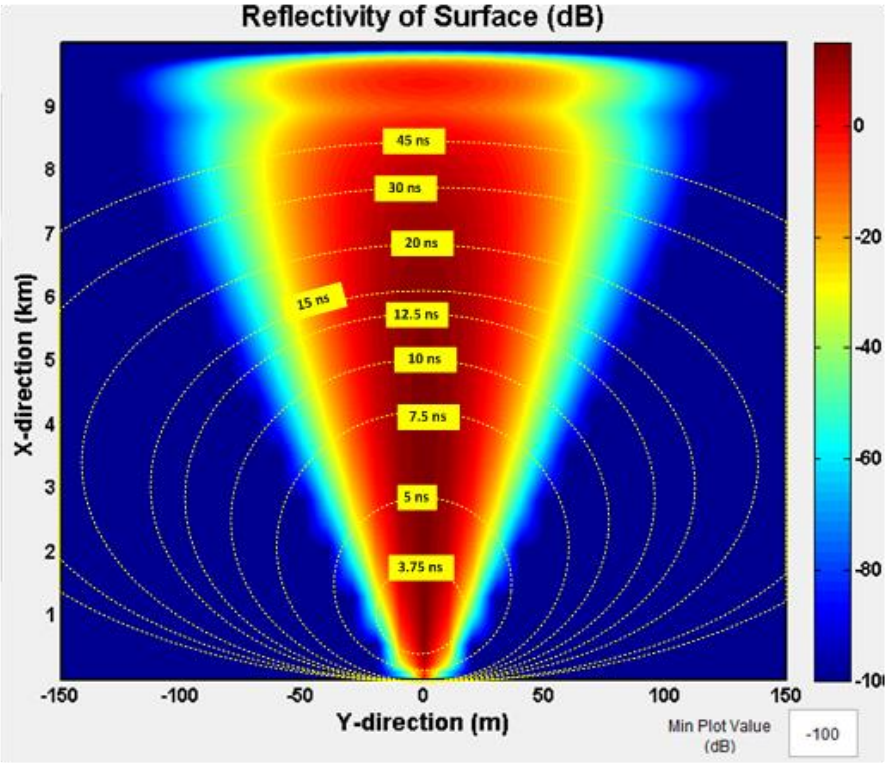

(a)

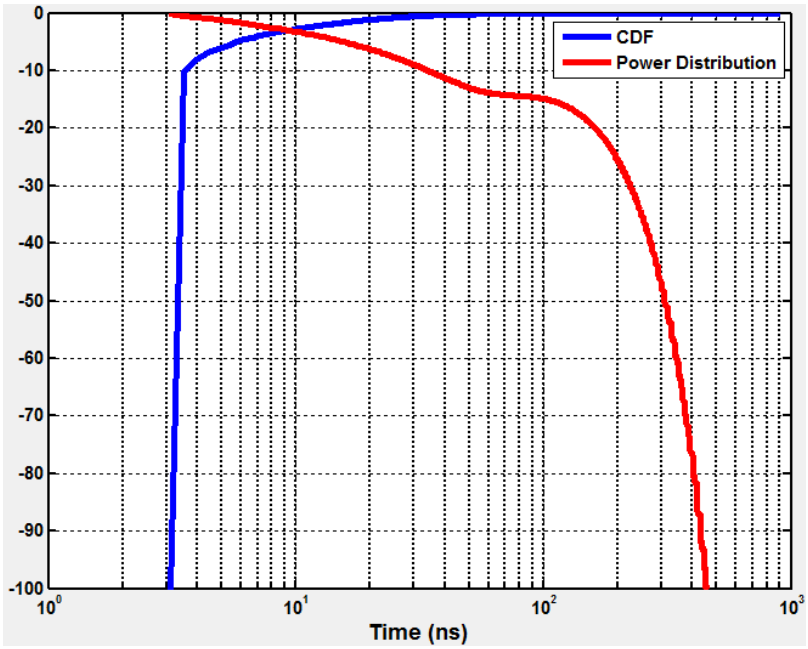

(b)

Figure 11: (a) Isolines to indicate regions of equal time (b) Power distribution vs. time

In this next example (Fig. 12a and 12b), the wide-angle scatter is also included. The surface is extended to ± 10 km in the y-direction to include the entire wide-angle scatter. With the wide-angle scatter included, reflected power returns arrive with delays as long as 10 ms! The returns with shorter delays are from the glistening region while the returns with longer delays are due to the wide-angle scatter (Fig. 12 b)

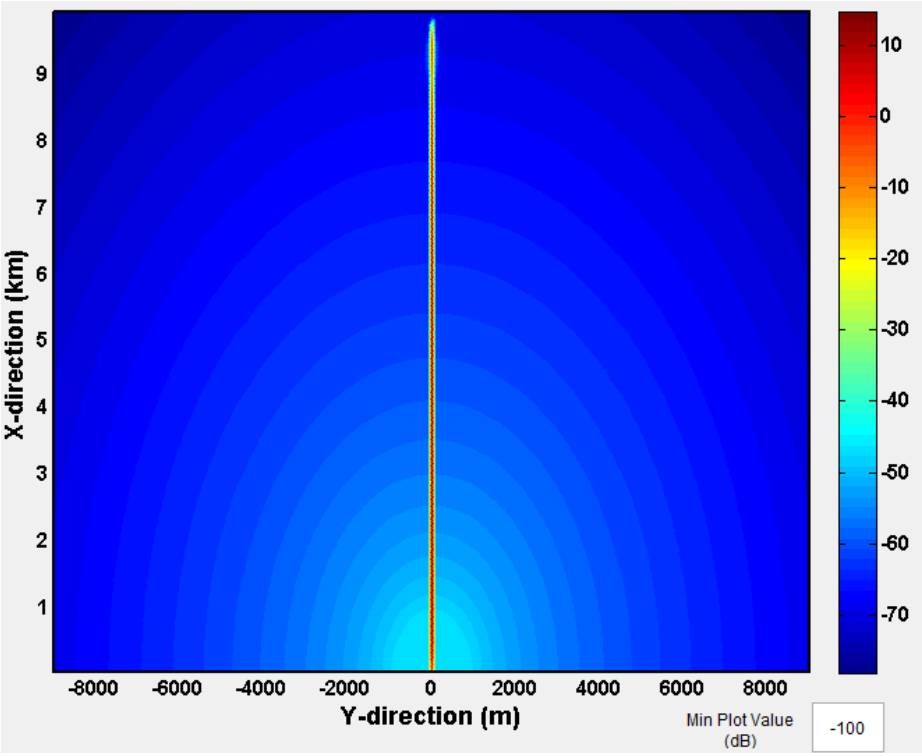

(a)

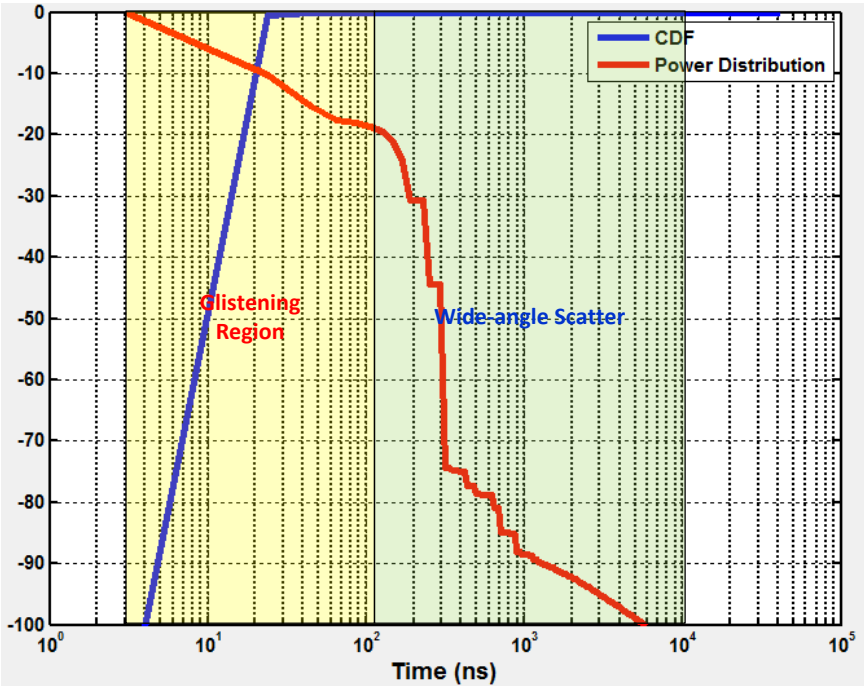

(b)

Figure 12 : (a) Bistatic surface reflectivity plot (b) Time vs. power plots

Finally, the effect of shadowing is shown via the surface reflectivity plots in Fig. 13. In this case, the focus is only at the glistening region.

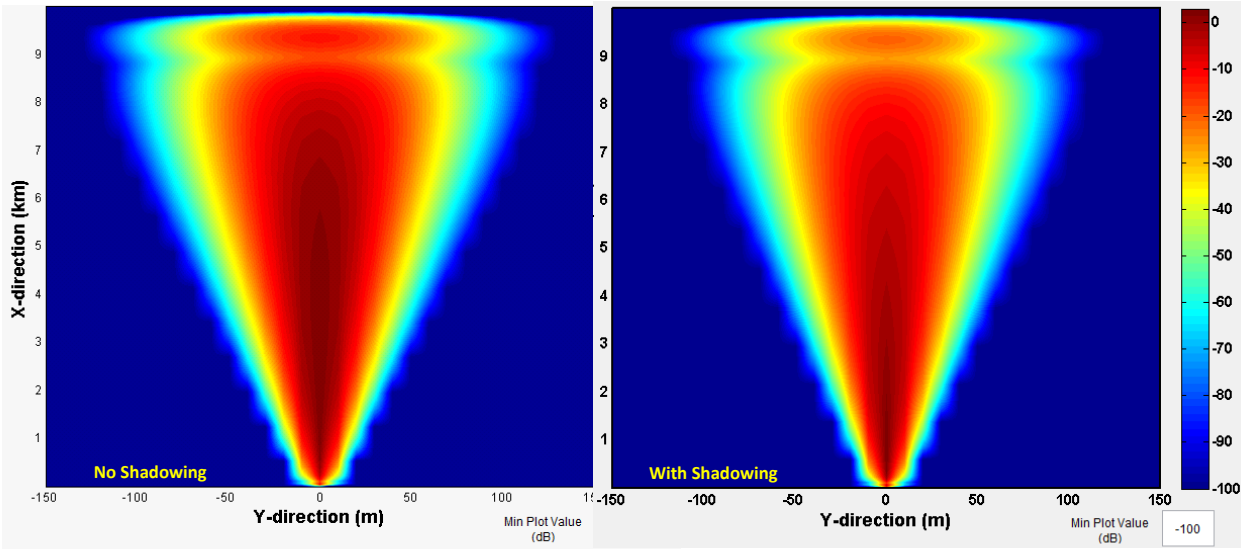

Figure 13: Comparing the change in the surface reflectivity in the glistening region with and without shadowing

2.2.7 Normalized Radar Cross-Section: Ducting Conditions

Given the complexity of modeling bistatic sea clutter reflectivity, as described in the previous Sections, with its superposition of three different physical processes, accounting for the effects of ducting could be complicated. Attempting to calculate bistatic sea reflectivity under ducting conditions in a manner analogous to that used for monostatic sea clutter, as discussed in Section 2.2.5 , where the "standard atmosphere" propagation factor is to be removed and the grazing angles are to be calculated using TEMPER, would not be straightforward. For these reasons, the computational steps required to handle ducting conditions are not included in the model.

3 COMPARISON WITH MEASURED DATA

Comparisons with measured data are essential to corroborate the theoretical model. Currently, limited data is available for comparison with the bistatic model especially in the glistening region. The most well-known are the experiments carried out by Beard [15] in 1961 between two antennas of equal height and about 3.5 km apart. Recently Haspert [16] has also made some low grazing angle measurements and compared his measured results to theory discussed by Barton [17]. Barton's theory is also based on Beckmann and Spizzichino. The biggest issue in making multipath measurements from the glistening zone is the small relative delay between the direct and multipath returns. These short delays demand use of narrow pulses with low sidelobes to enable resolution between direct and indirect returns. These narrow pulses need large bandwidths. The small differences in velocities between direct and indirect returns makes using Doppler difficult.

However, there is some measured data available in the wide-angle or backscatter region. The next section discusses comparisons with some examples of this data. There are no discussions of specular measurement comparisons as the developed model is primarily concerned with bistatic reflectivity results.

3.1 Pidgeon Data Set

In a 1965 paper by V.W. Pidgeon [12], an experimental program was carried out, where the bistatic radar cross section was measured as a function of transmitter and receiver depression angles. In Figure 14, two different lines are drawn. The "blue" curve (parametrically calculated by the authors) is the drawn over one of Pidgeon's data and its equation is:

$$\sigma^0 = -47 + 10\log_{10}\Psi_g \qquad (23)$$

where Ψ_g is the transmitter depression angle. This parametric equation is valid only for sea state 3 and vertical polarization. The NRL bistatic model is the basis for the "red" curve for increasing transmitter depression angle at sea state 3, vertical polarization and at C-Band.

The two curves show good agreement between the measured and modeled data. For example, at Ψ_g equal to 0.6^o, the experimental data predicts the bistatic RCS to be about -50dB while the NRL model predicts this value to be about -52dB.

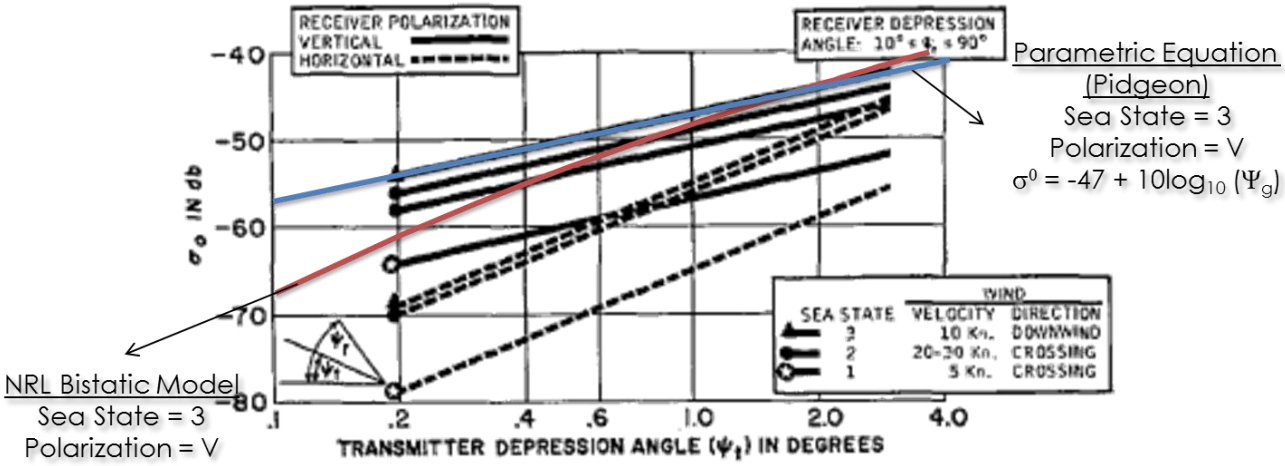

Figure 14: Summary of Bistatic Cross-section for Various Sea and Wind conditions; Transmitter Polarization: vertical; Frequency: C-band

3.2 Kochanski Data Set

A more recent paper (1992) by T. P. Kochanski [13], at M.I.T Lincoln Laboratory, summarizes measurements of bistatic sea backscatter at X-band (10GHz) using the Airborne Seeker Test bed and a CW (continuous wave) surface based illuminator. These measurements were made at sea state one and at vertical polarization. The transmitting antenna had a fixed depression angle while the depression angle of the receiving antenna located on an aircraft varied. The transmitter depression angle remained fixed at 0.3°. The receiver depression varied from 5° to 40°. The experimental data showed that the bistatic RCS was essentially independent of receiver depression angle.

Figure 15 shows the Kochanski experimental data overlaid with the results obtained using the NRL bistatic model. We observe the same independence from the transmitter depression angle in the NRL bistatic model. From the results, the average experimental bistatic RCS is about -50dB while, the NRL bistatic model puts this value at about -58dB. Once again, discounting for experimental errors, there is a reasonable match between experimental and modeled data.

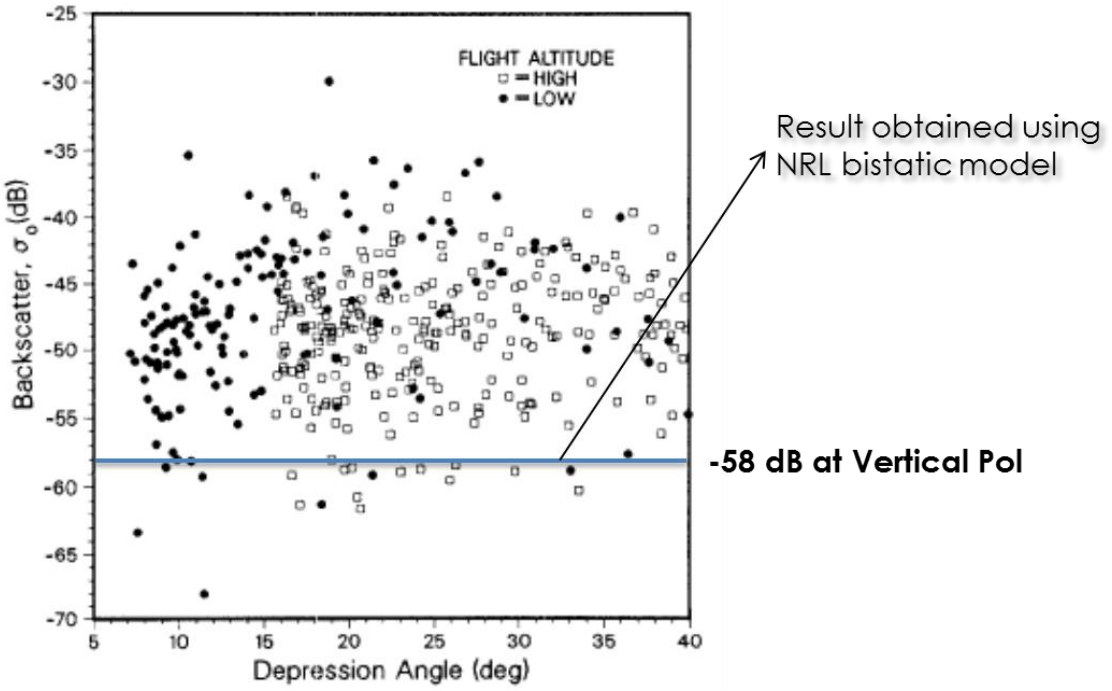

Figure 15: Comparing Kochanski's Experimental Results at X-band with Results Obtained using NRL Bistatic Model

3.3 Ewell Data Set

This 1982 publication by G. W. Ewell [14] describes experiments carried out at X-band for both horizontal and vertical polarization for a range of transmitter and receiver depression angles. The results plots the bistatic and monostatic RCS vs. the bistatic angle, defined as the angle between the receiver, the transmitter and the "aim point" between the two antennas as shown in figure 16. The data presents the ratio of the bistatic σ^o values and the monostatic σ^o values. Absolute values were not given, maybe because of an unreliable radar system calibration.

To get the data shown in figure 17, the transmitting antenna has a look direction of 90° in sea state 4. The separation distance between the receiving and transmitting antenna is at 3.5km. The height of the transmitting antenna is 22.9m while the height of the receiving antenna is at 8.2 m. Horizontal and vertical data was then taken for bistatic angles ranging from about 20° to 60°. Figure 17 shows the data calculated using the NRL bistatic model overlaid on the Ewell results for both the horizontal and vertical polarizations. For the three cases shown, the bistatic RCS is smaller than the monostatic RCS by about 10 dB. This is as expected since the monostatic RCS is based on the transmitter depression angle while the bistatic RCS is based on the smaller of the receiver and transmitter depression angle.

However, the results show that for most bistatic angles, the ratio of the bistatic RCS to the monostatic RCS from the NRL model never falls below -20dB, which is greater than the experimental data especially

at the larger bistatic angles. In the model, for the geometry shown in Fig. 6, Eq. (21) can be used to calculate both the monostatic and bistatic RCS with different α values. For the monostatic case, α is equal to the transmitter-grazing angle while for the bistatic case, α is equal to the smaller of the transmitter or the receiver-grazing angle. For most scenarios, the receiver is the smaller grazing angle. However, for no geometry is the receiver grazing angle so much smaller than the transmitter-grazing angle such the ratio of the bistatic to the monostatic RCS falls much less than 10 dB for fixed frequency, polarization and sea state. Hence, further analysis may be necessary to understand the discrepancy between the measured and modeled data for this case.

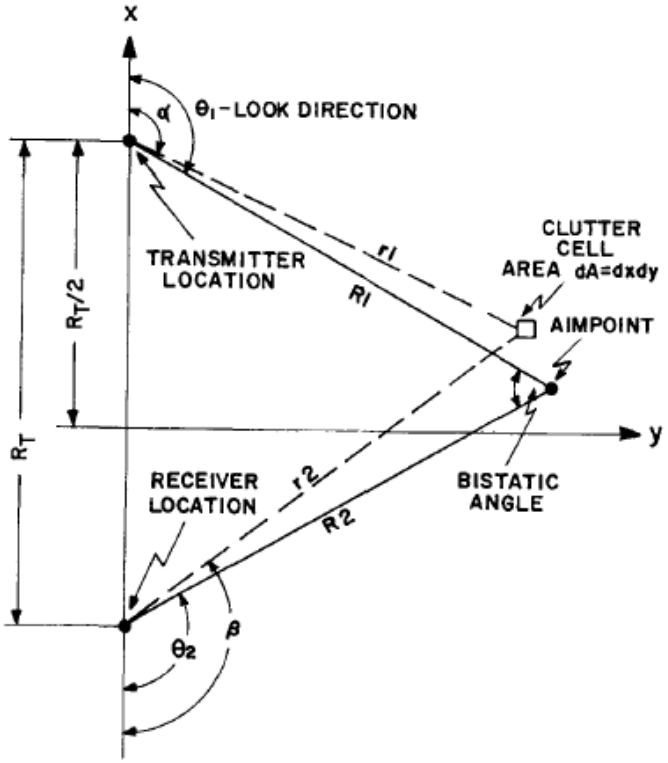

Figure 16: Geometry and Nomenclature for the Ewell Experiment [14]

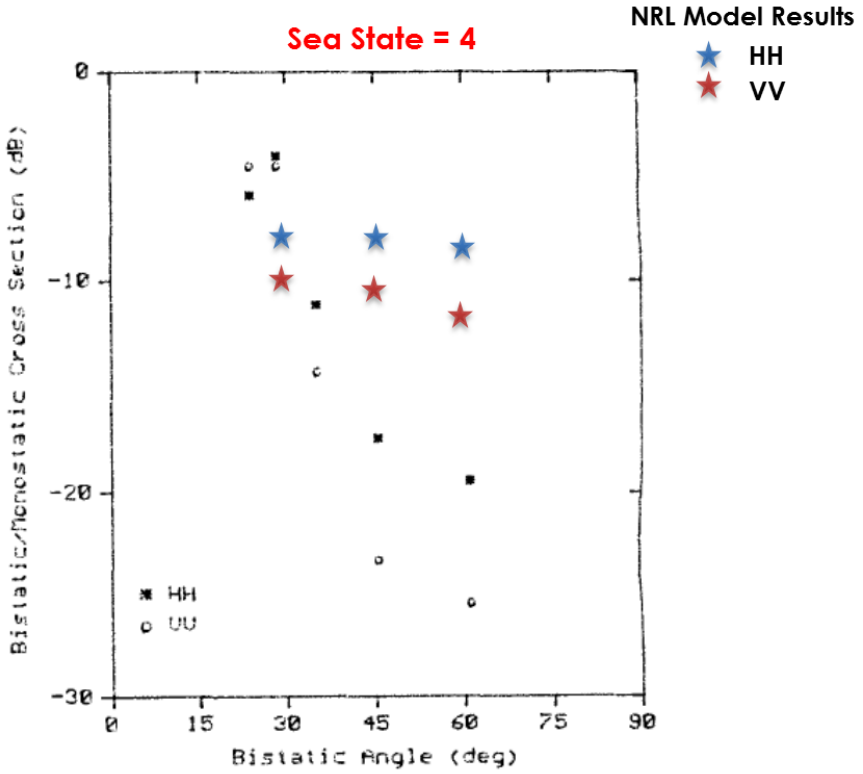

Figure 17: Comparison of Ewell Experimental Data with the NRL Bistatic Model Data

4 CONCLUSIONS

Modeling of bistatic sea surface reflectivity is a complex problem due to the many parameters defining the geometry of interest. The current state of the art invokes three different components: coherent scatter (reflection) from the specular region, strong directive diffuse scatter from the glistening region, and wide angle diffuse scatter in directions outside the glistening region. The report describes in detail the steps used to model the diffuse scatter assuming a Gaussian sea surface model. This basis of this geometrical model is primarily the work done by Beckmann and Spizzichino in the 1960s. Currently, there is a serious lack of a mature bistatic sea reflectivity model because of limited measured bistatic sea clutter data to seriously anchor any modeling attempts. There are still many unknown issues related to monostatic sea clutter, for example sea spikes, which will certainly impact bistatic clutter modeling, and which are still very much under active research. The model presented here represents the best available theory but uncertainties must nevertheless be associated with any quantitative results obtained.

5 REFERENCES

[1] P.Beckmann and A.Spizzichino, **The Scattering of Electromagnetic Waves from Rough Surfaces**, New York:Pergamon Press, 1963.

[2] R.J.Wagner, "Shadowing of randomly rough surfaces", Journal of Acoustical Society of America, Vol.41 1967.

[3] K.M.Mitzner, "Change in polarization on reflection from a tilted surface", RadioScience, Vol.1 1966.

[4] G.D.Dockery, "Method for modelling sea surface clutter in complicated propagation environments", IEE Proc.F, Communications, Radar & Signal Processing, Vol.137, pp. 73-79, April, 1990.

[5] G.D.Dockery, "Modeling electromagnetic wave propagation in the troposphere using the parabolic equation", IEEE Transactions on Antennas and Propagation, Vol.AP-36, pp. 1464-1470, October, 1988.

[6] L.V.Blake, **Radar Range-Performance Analysis**, Norwood, MA:Artech House,2, 1986.

[7] B.G.Smith, "Geometrical shadowing of a random rough surface", IEEE Transactions on Antennas and Propagation, Vol.AP-15 1967.

[8] C.Bourlier and G.Berginc, "Shadowing function with single reflection from anisotropic Gausiian rough surface. Application to Gaussian, Lorentzian, and Sea Correlations", Waves in Random Media, Vol.13 2003.

[9] V.Gregers-Hansen and R.Mital, "An empirical sea clutter model for low grazing angles", RadarCon09, Pasadena, CA, pp. 1-5, May 4, 2009.

[10] F.E.Nathanson, et al, **Radar Design Principles**, New York:McGraw-Hill,2, 1991.

[11] V.Gregers-Hansen and R.Mital, "An Empirical Sea Clutter Model for Low Grazing Angles", 2009 IEEE Radar Conference, RadarCon09, pp. 61-65, May 4, 2009.

[12] V.Pidgeon, "Bistatic cross section of the sea", IEEE Trans.on Antennas and Propagation, Vol.AP-14, pp. 405-406, May, 1966.

[13] T.P.Kochanski, et al, "Low illumination angle bistatic sea clutter measurements at X-band", IEE Int. Conf. Oceans '92 Mastering the Oceans Through Technology, Newport,RI, October 26, 1992.

[14] G.W.Ewell and S.P.Zehner, "Bistatic sea clutter return near grazing incidence", International Radar Conference RADAR-82, London,UK, October, 1982.

[15] C. I. Beard, "Coherent and Incoherent Scattering of Microwaves from the Ocean", IRE Transactions on Antennas and Propagation, vol. AP-5, pp. 183 - 191, 1957.

[16] K. Haspert and M. Tuley, "Comparison of Predicted and Measured Multipath Impulse Responses", IEEE Transactions on Aerospace and Electronic Systems, vol. 47, no, 3, pp. 1696 - 1709, July 2011.

[17] D. K. Barton, "Low-angle radar tracking", Proceedings of the IEEE, vol. 62, no. 6, pp. 687-704, June 1974.

Appendix A - MATLAB IMPLEMENTATION OF BISTATIC MODEL

A MATLAB function was written to compute the bistatic sea reflectivity for a given set of parameters. This function will calculate the average horizontal and vertical bistatic reflectivity for a specified surface patch. With reference to the program listing shown below as Figure 1 the inputs are as follows:

1. Height of the receiving antenna (h_R) in meters
2. Angle of elevation (θ_d) to the transmitting antenna
3. Sea State (SS)
4. Distance between the receiving and transmitting antennas (D) in meters
5. Frequency of operation ($FGHz$) in GHz
6. The x-coordinate of the surface patch in meters
7. The y-coordinate of the surface patch in meters
8. Indicate whether shadowing is to be applied or not
9. Indicate the polarization of the incident ray (choose between Horizontal or Vertical)

The outputs of this code are the following:

1. The average co-pol and cross-pol surface reflectivity for the given x- and y-coordinates in dB
2. The angle from the receiver horizontal to the surface patch (ϕ_{Rx})
3. The angle from the transmitter horizontal to the surface path (ϕ_{Tx})
4. The off-axis angle from the receiver to the surface patch (θ_1)
5. The off-axis angle from the transmitter to the surface patch (θ_2)
6. Grazing angle from receiver (γ_R)
7. Grazing angle from transmitter (γ_T)
8. Length of path from receiver to surface patch (R_1) in meters
9. Length of path from transmitter to surface patch (R_2) in meters
10. Direct path length between receiver and transmitter (R_d) in meters
11. Height of transmitting antenna (h_T) in meters

The main report defines the equations used in this MATLAB® listing.

```
function[sigmaCoPol_dB, sigmaXPol_dB,...
   grazRx, grazTx, phiRx, phiTx, thetaRx, thetaTx, R1, R2, Rd, hT] = ...
   ReflectivityCoeff_Calculation(hR, thetad, SeaState, D, FGHz, xPatch, yPatch, Shadowing, TxPol, Type,hT)

clc;

%% CONSTANTS
Deg2Rad = pi/180;
SpeedofLight = 3e8;
Re = 8500e3;

if nargin == 0
   hR = 20;
   D = 10e3;
   thetad = 3.0;
   SeaState = 3;

   xPatch = 50;
   yPatch = 0;

   FGHz = 3;

   Shadowing = 'Y';
   TxPol = 'V';

   Type = 1;

end;

%Define slope from Sea State

if SeaState == 0
   tanbeta0 = 0.05;
elseif SeaState == 1
   tanbeta0 = 0.12;
elseif SeaState == 2
   tanbeta0 = 0.14;
elseif SeaState == 3
   tanbeta0 = 0.15;
elseif SeaState == 4
   tanbeta0 = 0.16;
elseif SeaState == 5
   tanbeta0 = 0.18;
elseif SeaState == 6
   tanbeta0 = 0.22;
elseif SeaState == 7
   tanbeta0 = 0.25;
end;

%Electrical properties of sea water
lambda = SpeedofLight/(FGHz*1e9);
epsrc = 80 - 60 * sqrt(-1) * lambda * 4;
murc = 1;
```

```
YEarth = sqrt(epsrc/murc);



%% START CALCULATION OF SURFACE REFLECTIVITY
alpha = D/Re;
TD = thetad * Deg2Rad;
 %Calculate the height of Transmitter
if Type == 1
   beta = pi - (TD + pi/2) - alpha;
   hT = ((Re + hR) * sin(TD + pi/2)/ (sin(beta))) - Re;

end;
Rd = sqrt((hT - hR)^2 + 4*(Re+hR)*(Re+hT)*sin(alpha/2)^2);

x1 = sqrt(xPatch^2 + yPatch^2);
alpha1 = x1/Re;

if xPatch == 0
   theta4 = 0;
elseif xPatch < 0
   theta4 = pi/2 + acos(xPatch/x1);
else
   theta4 = acos(xPatch/x1);
end;

thetaRx = theta4/Deg2Rad;

x2 = sqrt(x1^2 + D^2 - 2 * x1 * D * cos(theta4));
theta3 = acos((x2^2 + D^2 - x1^2)/(2 * x2 * D));

thetaTx = theta3/Deg2Rad;



alpha2 = x2/Re;

R1 = sqrt(hR^2 + 4 * Re * (Re + hR) * sin(alpha1/2)^2);
R2 = sqrt(hT^2 + 4 * Re * (Re + hT) * sin(alpha2/2)^2);

%Calculate grazing and incidence angles from receiver hR
verth1 = (hR + Re) - (Re/cos(alpha1));
horzh1 = Re * tan(alpha1);

graz1 = acos((R1^2 + horzh1^2 - verth1^2) / (2 * R1 * horzh1));



if isnan(graz1)
   graz1 = pi/2;
end;

%Grazing angle from reflecting surface to Receiver
grazRx = graz1/Deg2Rad;

theta1 = pi/2 - graz1;
```

```
%Angle from Rx horizontal to Reflecting surface
phiRx = 90 - acos(((Re+hR)^2 + R1^2 - Re^2)/(2 * R1 * (Re+hR)))/Deg2Rad;

verth2 = (hT + Re) - Re/(cos(alpha2));
horzh2 = Re * tan(alpha2);

graz2 = acos((R2^2 + horzh2^2 - verth2^2)/(2 * R2 * horzh2));

if isnan(graz2)
   graz2 = pi/2;
end;

%Grazing angle from reflecting surface to Transmitter
grazTx = graz2/Deg2Rad;

theta2 = pi/2 - graz2;

%Angle from Tx horizontal to Reflecting surface
phiTx = 90 - acos(((Re + hT)^2 + R2^2 - Re^2)/(2 * R2 * (Re + hT)))/Deg2Rad;



if yPatch < 0
   totAngle = abs(theta4) + theta3;
else
   totAngle = 2 * pi - (abs(theta4) + theta3);
end;

tanbeta = sqrt(sin(theta1)^2 - 2 * sin(theta1) * sin(theta2) * cos(totAngle) + sin(theta2)^2) / ...
   (cos(theta1) + cos(theta2));

if strcmpi(Shadowing,'Y') ==1
   v1 = abs(cot(theta1))/(sqrt(2)*tanbeta0);
   v2 = abs(cot(theta2))/(sqrt(2)*tanbeta0);

   B1 = (exp(-v1 * v1) ./ v1 - sqrt(pi) * erfc(v1)) ./ (2 * sqrt(pi));
   B2 = (exp(-v2 * v2) ./ v2 - sqrt(pi) * erfc(v2)) ./ (2 * sqrt(pi));

   Shadow_Factor = (1 + erf(v1)) * (1 + erf(v2)) ./ (4 .* (1 + B1 + B2));
else
   Shadow_Factor = 1;
end;

if verth1 > 0 && verth2 > 0
   temp1 = (1+tanbeta^2)^2/(tanbeta0^2) * exp(-(tanbeta/tanbeta0)^2);
   temp1 = temp1 * Shadow_Factor;

   %Calculate alpha -- to include Polarization
   alpha = acos((sqrt(1 - cos(graz1)*cos(graz2)*cos(totAngle) + sin(graz1)*sin(graz2)))/sqrt(2));
   Alpha = pi/2 - alpha;

   if strcmpi(TxPol,'H') ==1
      RHoriz = (sin(Alpha) - sqrt(YEarth^2 - cos(Alpha)^2)) ...
```

```
        / (sin(Alpha) + sqrt(YEarth^2 - cos(Alpha)^2));

    elseif strcmpi(TxPol,'V') ==1
        RVert = (YEarth^2 * sin(Alpha) - sqrt(YEarth^2 - cos(Alpha)^2)) ...
            / (YEarth^2 * sin(Alpha) + sqrt(YEarth^2 - cos(Alpha)^2));

    end;

    cosX = cos(theta1) * cos(theta2) - sin(theta1) * sin(theta2) * cos(totAngle);
    sinX = sqrt(1-cosX^2);

    sinbeta1 = sin(theta1) * sin(totAngle) / sinX;
    sinbeta2 = sin(theta2) * sin(totAngle) / sinX;

    cosbeta1 = (sin(theta2) * cos(theta1) + cos(theta2) * sin(theta1) * cos(totAngle))/sinX;
    cosbeta2 = (sin(theta1) * cos(theta2) + cos(theta1) * sin(theta2) * cos(totAngle))/sinX;

    if strcmpi(TxPol,'H') == 1
        sigmaCoPol =temp1 * real((abs(RHoriz) * cosbeta1 * cosbeta2)^2);
        sigmaXPol = temp1 * real((abs(RHoriz) * cosbeta1 * sinbeta2)^2);

    elseif strcmpi(TxPol,'V') == 1
        sigmaCoPol = temp1 * real((abs(RVert) * cosbeta1 * cosbeta2)^2);
        sigmaXPol = temp1 * real((abs(RVert) * cosbeta1 * sinbeta2)^2);
    end;



    %Have to include Monostatic for wide angle scattering
%     if xPatch < 0
%         graz = grazRx;
%     else
        graz = min(grazRx,grazTx); %Choose the smaller of the two grazing angles
%     end;
    if strcmpi(TxPol,'H') ==1
        CC1 = -73.0;  CC2 = 20.781; CC3= 7.351; CC4=25.65; CC5 = 0.0054;
    elseif strcmpi(TxPol,'V') ==1
        CC1 = -50.796; CC2 = 25.93; CC3 = 0.7093; CC4 = 21.588; CC5 = 0.00211;
    end;
    temp2 = CC1 + CC2 * log10(sin(graz*Deg2Rad)) + ...
        (27.5 + CC3 * graz) * log10(FGHz)/(1.0 +0.95 * graz) + ...
        CC4 * (SeaState + 1) ^ (1/(2.0 + 0.085 * graz + 0.033 * SeaState)) + CC5*graz.^2;

    temp2 = 10^(temp2/10);

    A = [sigmaCoPol, temp2];
    sigmaCoPol = max(A);

    A = [sigmaXPol, 0];
    sigmaXPol = max(A);
else
    sigmaCoPol = 0;
    sigmaXPol = 0;
end;
```

```
%Co- and X-Pol Bistatic RCS in dB

sigmaCoPol_dB = 10.*log10(sigmaCoPol);
sigmaXPol_dB = 10.*log10(sigmaXPol);

if sigmaCoPol_dB <= -80
   sigmaCoPol_dB = -80;
end;

if sigmaXPol_dB <= -80
   sigmaXPol_dB = -80;
end;
```

Figure A.1: MATLAB Listing for Calculation of Average Sea Reflectivity using Geometric Bistatic Model

Appendix B - MATLAB GRAPHICAL USER INTERFACE (GUI) FOR BISTATIC CALCULATIONS

The MATLAB function described in Appendix A was used to construct a Graphical User Interface (GUI) to provide a convenient way to use the code for a given surface geometry. This MATLAB program determines the basic reflectivity, the bistatic RCS, as well as received power and time delay distribution.

The inputs to the GUI include:

- Frequency of operation in GHz
- Transmit and receive polarization
- Range in km between receiver and transmitter
- Height of receiver in meters
- Elevation angle to transmitter
- Gain and sidelobe level of receiving antenna, which has a Gaussian shape and a constant sidelobe level. The transmit antenna is isotropic
- Sea-state can be chosen as shown in Table 1
- The calculations are based on the user input of flat or spherical earth
- The option of including shadowing and/or wide-angle scatter is available
- The resolution of the plot as well the size of the surface can also be specified

The code outputs the maximum scattered power and determines the diffused scattering coefficient. It also plots as output

- The glistening surface
- The average bistatic RCS depending on unit patch size
- The apparent bistatic RCS which includes the effect of gain of the main beam of the receiving antenna,
- The average diffused power from the surface depending on individual patch sized defined by user
- Time vs. power plots which indicates the delay of the diffused power from the surface as it reaches the receiving antenna. This is very important when determining the degradation in the sidelobe canceller because scattered power with high delays cannot be easily cancelled by an adaptive canceller
- Range vs. power plots, which allow the user to determine at which range most diffused power comes from.

Figure B.1 shows the GUI for the MATLAB® code and Figure B.2 shows examples of results produced by the code. All code is available from NRL upon request.

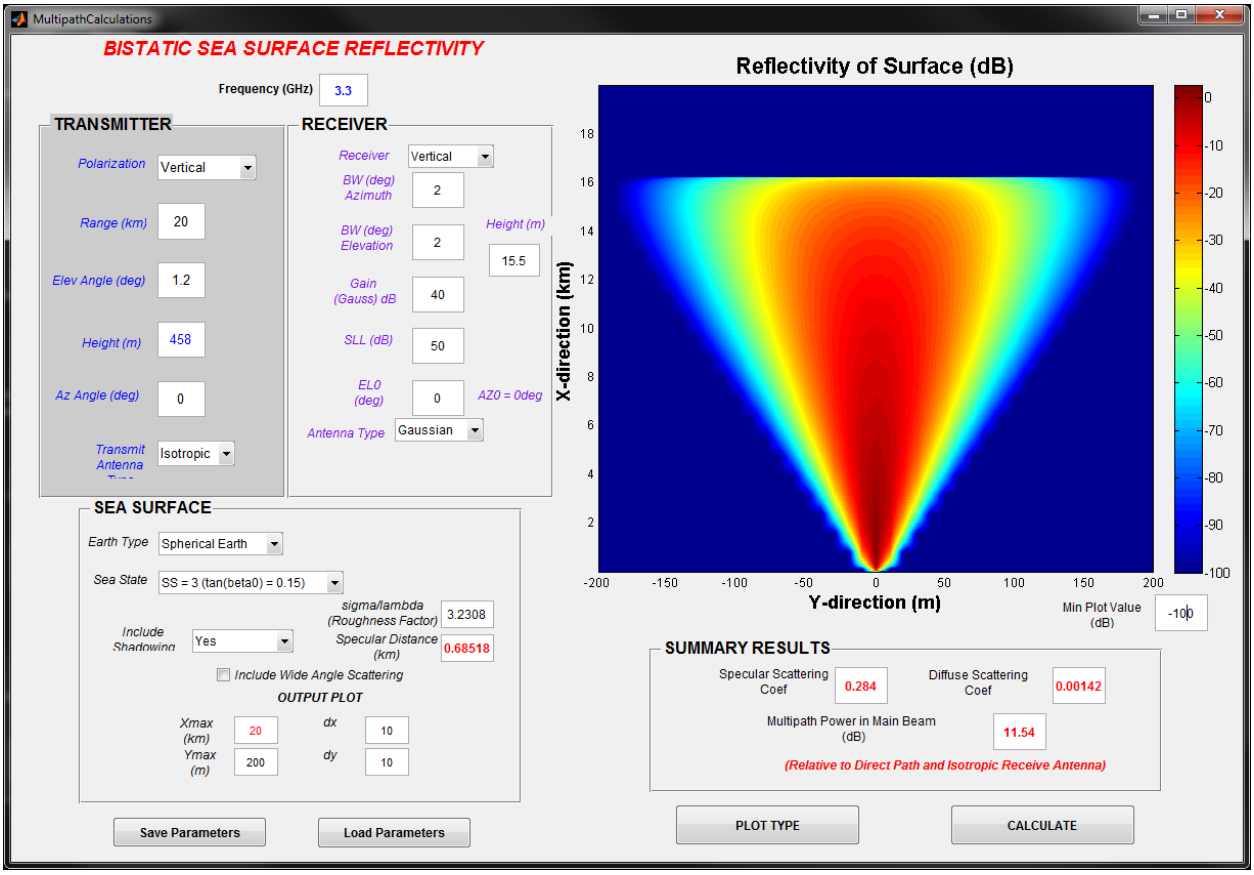

Figure B.1: MATLAB GUI (Graphical User Interface) to determine diffuse power from a planar surface for a given geometry

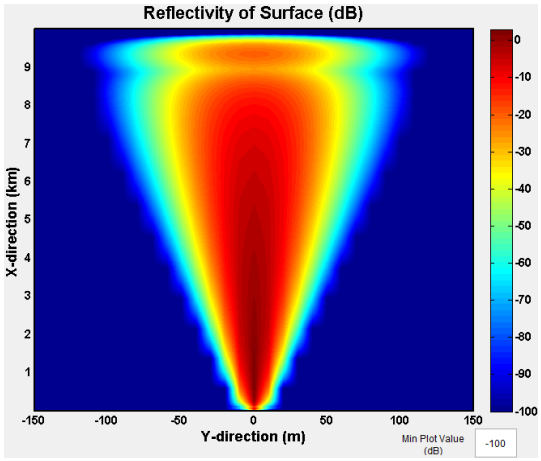

- This plot shows the bistatic RCS over the entire surface of interest
- The equation used for this plot is Equation (10) of the main report
- The plot is limited due to the horizon

(a) Reflectivity of Surface

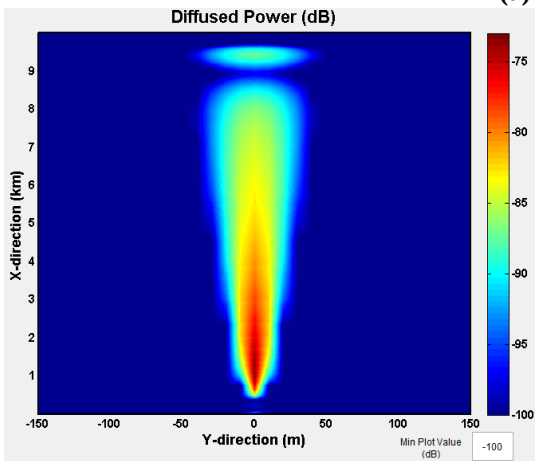

- In this plot, the gain of the transmit and receive antennas are also included
- Most of the diffused power comes from close to the receive antenna where the delays can be quite long

(b) Diffuse Power over Given Surface

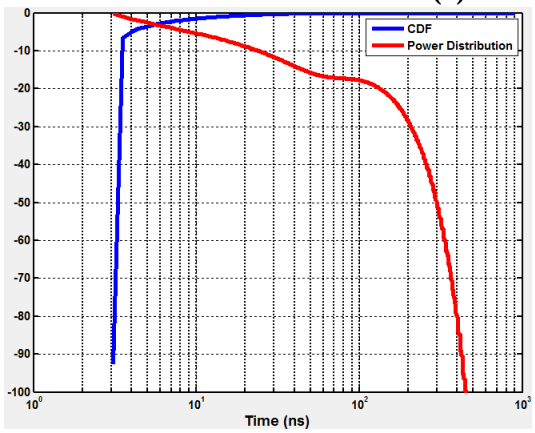

- This is cumulative distribution plot of the incoming power vs. time (ns)
- The power numbers have been normalized to the maximum incoming power
- In this case more than 50% of the power has delays greater than 3ns (since no wide-angle scatter) has been

(c) Plot of fractional power vs. time (ns)

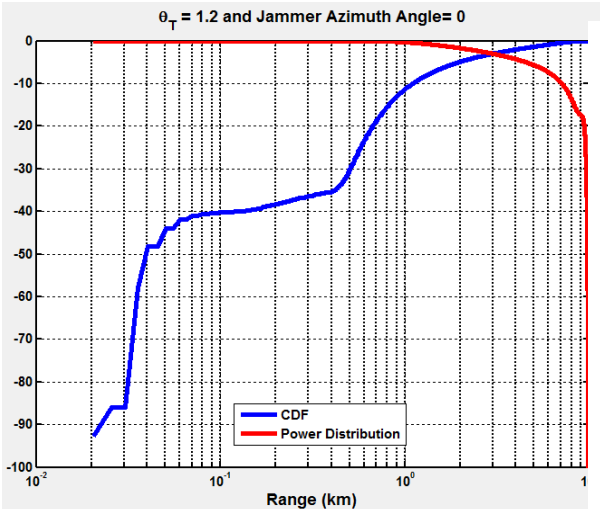

- This is cumulative distribution plot of the incoming power vs. range (km)
- The power numbers have been normalized to the maximum incoming power
- This plot allows the user to understand the range from which most of the power is coming from

(d) Plot of fractional power vs. range (km)

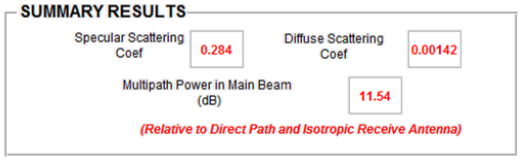

- The tab gives a summary of the results calculated by the program
- Specular coefficient
- Diffuse scattering coefficient
- Maximum multipath power

(e) Summary of results

Figure B.2: Example of results available from "Bistatic Sea Surface Reflectivity" Code